JOURNAL OF AEROSOL MEDICINE AND PULMONARY DRUG DELIVERY
Volume 21, Number 4, 2008

Pp. 335–341
DOI: 10.1089/jamp.2008.0698

# MRI Measurement of Regional Lung Deposition in Mice Exposed Nose-Only to Nebulized Superparamagnetic Iron Oxide Nanoparticles

Andrew R. Martin, Ph.D.,[1] Richard B. Thompson, Ph.D.,[2] and Warren H. Finlay, Ph.D.[1]

## Abstract

Superparamagnetic iron oxide nanoparticles show potential in magnetic targeting of inhaled aerosols to localized sites within the lung. These particles are also used as contrast agents in magnetic resonance imaging (MRI). In the present work, we examine the feasibility of measuring regional lung deposition of iron oxide nanoparticles using MRI. Mice were exposed nose-only to nebulized superparamagnetic iron oxide nanoparticles. The droplet size distribution in the inhalation chamber was measured using a time-of-flight device. Regional concentrations of iron in the left and right lung were assessed with MRI by measuring the longitudinal relaxation times ($T_1$) of the lung tissue in exposed mice, compared to a baseline group. Regional concentrations of iron in the lungs of the mice ranged from $1.1 \pm 0.8$ $\mu g/cm^3$ (mean $\pm$ one standard deviation, $n = 6$) in peripheral lung regions to $2.7 \pm 1.4$ $\mu g/cm^3$ in the central lung, with no significant difference between the left and right lung. The nebulized droplets in the inhalation chamber had mass median aerodynamic diameter (MMAD) of $5.6 \pm 0.8$ $\mu m$, with a geometric standard deviation (GSD) of $1.30 \pm 0.03$ (both values expressed as mean $\pm$ one standard deviation, $n = 6$). MRI shows promise for *in vivo* measurement of regional lung concentrations of superparamagnetic iron oxide nanoparticles, and may be useful in studies of lung deposition and clearance.

**Key Words:** magnetic resonance imaging, lung deposition, mice; nose-only inhalation, superparamagnetic iron oxide nanoparticles, MRI, SPIONs

## Introduction

The potential use of magnetic fields to influence regional lung deposition of inhaled pharmaceutical aerosols has gained considerable attention recently.[1,2] Superparamagnetic iron oxide nanoparticles have been used to imbue aerosol particles with high magnetic susceptibility, allowing their trajectories[3] and orientations[4] to be controlled at a distance using magnetic fields. Recent work[5] has also indicated that magnetic control over aerosol particle shape may be possible. Although considerable hurdles remain before such technologies find clinical application, the ability to noninvasively enhance aerosol deposition at localized sites within the lung, using externally applied magnetic fields, would be a significant step forward in respiratory drug delivery.

In addition to their potential use in targeting drug delivery, iron oxide nanoparticles are widely used as contrast agents for magnetic resonance imaging (MRI).[6,7] Accordingly, for the intravenous route of administration, iron oxide nanoparticles have been used for combined magnetic targeting and subsequent, MRI-based assessment of nanoparticle concentrations within targeted sites in both clinical trials[8] and animal models.[9] Very recently, Sood et al.[10] have used MRI to estimate gadolinium concentrations averaged over the entire lungs of newborn pigs exposed to nebulized solutions containing gadopentetate dimeglumine (Gd-DTPA). In the present work, we examine the possibility that MRI might be used to determine the distribution of inhaled iron oxide nanoparticles within the lung. Clearly, measurement of regional deposition patterns by MRI would be ideally suited for *in vivo* evaluation of magnetic drug targeting techniques employing aerosols loaded with iron oxide nanoparticles. The ability to noninvasively quantify the

[1]Department of Mechanical Engineering, University of Alberta, Edmonton, Alberta, Canada.
[2]Department of Biomedical Engineering, University of Alberta, Edmonton, Alberta, Canada.

level of targeting achieved in individual patients would be of great benefit, providing researchers with direct feedback on the success or failure of novel magnetic targeting techniques, and enabling correlations to be established between deposition enhancement at targeted sites and clinical outcomes.

Animal models have been widely used in aerosol inhalation studies, and regional deposition patterns are qualitatively similar in laboratory animals and humans.[11] In the work decribed at present, mice were exposed nose-only to nebulized droplets containing superparamagnetic iron oxide nanoparticles. The feasibility of measuring lung concentrations of iron oxide nanoparticles using MRI was assessed by comparing lung tissue $T_1$ relaxation times of exposed mice with those of baseline, nonexposed mice. Regional variation in deposition was assessed by comparing iron concentrations in the left and right lung measured in different axial slices.

## Materials and Methods

### *Materials and animals*

Colloidal superparamagnetic iron oxide with an iron concentration of 10 mg/mL, and reported core particle size of 10 nm was purchased (FeREX; BioPAL, Worcester, MA). Six- to 8-week-old female BALB/c mice were obtained from the Health Sciences Laboratory Animal Services at the University of Alberta. The mice were housed under conventional conditions under the guidelines of the Canadian Council on Animal Care for 1 week prior to the study. All animal procedures were approved by the University of Alberta Health Sciences Animal Policy and Welfare Committee.

### *Aerosol exposure*

The aerosol exposure apparatus used in the present study was nearly identical to that used previously by Nadithe et al.[12] Briefly, LC Star jet nebulizers (PARI GmbH, Starnberg, Germany), operated with Devilbiss PulmoAide compressors (American Allergy Supply, Houston, TX), were used to supply droplets containing colloidal iron oxide nanoparticles to a nose-only inhalation chamber. The vents of the nebulizers were sealed to prevent additional room air from being drawn into the system. The downstream side of the inhalation chamber was connected to a house vacuum in order to maintain atmospheric pressure inside the chamber. Prior to the exposure, the output rate of colloidal iron oxide from the nebulizers was determined by placing three Respirgard filters (Vital Signs, Totowa, NJ) in series at the nebulizer exit. Nebulization was allowed to proceed until completion, and then the filters were weighed to determine the mass of aerosol generated. In addition, the droplet size distribution inside the chamber was also determined, prior to the exposure, using an Aerosizer (Amherst Process Instruments; now TSI, Shoreview, MN) to sample aerosol from the nose ports of the chamber, at a sampling flow rate of 1 L/min. Aerosol was sampled from the six ports later occupied, during the exposure, by mice.

Six mice, weighing 22.5 ± 1.2 g (mean ± 1 standard deviation), were placed inside restrainer tubes and exposed to nebulized iron oxide for 2 h. Due to the length of the exposure, the nebulizer and compressor were switched out of the circuit and replaced two times. Each time, flow of air through the chamber was maintained using the house vacuum, and less than 2 min elapsed before the new nebulizer and compressor were in place and again producing aerosol. The mice were euthanized immediately after the exposure by intraperitoneal injection of euthanyl, and then placed in a refrigerator at 4°C, in supine position, until the time of their MRI scans. The time of death and the time of MRI scan was recorded for each mouse. The scan of the first exposed mouse began approximately 1 h after euthanization.

In addition to the exposed mice, a group of six baseline mice was studied, with a mean weight of 22.8 ± 0.3 g. Two of these mice underwent a blank 2-hr exposure to isotonic saline, after which they were euthanized together with the remaining four baseline mice, and then all six baseline mice were refrigerated until scanned. As for the exposed mice, times of death and scanning were recorded for each mouse.

### *MRI imaging and postprocessing*

All MRI measurements were performed on a Siemens Sonata 1.5T 60-cm bore system (Siemens Medical Systems, Erlangen, Germany). All mice were oriented prone, in the right to left direction, in a 2.5-cm diameter surface coil, with the center of the lung placed at the center of the circular coil to maximize reception sensitivity and uniformity over the lung. An inversion-recovery fast spin echo pulse sequence with a variable inversion time ($T_i$ = 200 ms: 200 ms:2000 ms, and $T_i = \infty$) was used to quantify the longitudinal relaxation time of the lungs, using the following parameters: 108 × 25 mm field of view, 448 × 105 matrix (240 × 240 $\mu$m in-plane spatial resolution, interpolated to 120 × 120 $\mu$m), and 1-mm slice thickness with 12 slices spanning the lung from the trachea down to the diaphragm. Two serial experiments, each with six slices with a 1-mm slice gap, were interleaved to ensure there was no crosstalk between neighboring slices. Other pulse sequence parameters included a repetition time, *TR*, of 4000 ms, an echo time, *TE*, of 16 ms, a 150-Hz/pixel bandwidth, a 15.9-ms echo-space with 11 echoes per excitation, and two averages. The total acquisition time per mouse was approximately 30 min.

A MATLAB (The Mathworks, Natick, MA) script was written to calculate average $T_1$ relaxation times for user-defined regions of interest within the slices. For the analysis reported here, regions of interest encompassing the left and right lung were chosen in each slice. To limit the influence of the lung vasculature on $T_1$ relaxation times, all voxels with signal intensity greater than a threshold value were excluded from the regions of interest. A threshold level equal to 25% of the maximum signal intensity in an image was found to filter out the majority of the vasculature visible in the image. In addition, the average signal intensity (*SI*) in each region of interest was corrected for noise using the relationship

$$SI = \sqrt{SI_0^2 - n^2} \quad (1)$$

where $SI_0$ is the average signal intensity prior to subtraction of the noise, $n$, measured as the average signal intensity in a region of interest far away from the mouse.

The $T_1$ relaxation time was determined in each region of interest by fitting average signal intensity versus inversion time data points with the function

$$SI = \text{abs}\left|SI_\infty\left(1 - k\cdot e^{-T_i/T_1}\right)\right| \quad (2)$$

where $SI$ is the signal intensity at inversion time $T_i$, and the constants $SI_\infty$, k, and $T_1$ were determined by nonlinear regression.

The presence of iron oxide nanoparticles in the lung will decrease the $T_1$ relaxation time according to the following relationship:[13,14]

$$\frac{1}{T_1} = \frac{1}{T_{10}} + \alpha\cdot c \quad (3)$$

where $T_{10}$ is the baseline relaxation time, $c$ is the tissue concentration of iron, and $\alpha$ is ideally a constant and is the relaxivity of the particles. Evaluation of Equation (3) allowed the average concentration of iron within chosen regions of interest to be calculated from measured $T_1$ relaxation times in the exposed and baseline mice. For the iron oxide nanoparticles used in the present study we derived a value of $\alpha$ = 0.15 $cm^3/(\mu g\ Fe\cdot s)$ by evaluating Equation (3) using known concentrations of the nanoparticles prepared in agar phantoms along with the corresponding $T_1$ and $T_{10}$ values measured using inversion recovery MRI experiments. The phantoms contained 2% (w/v) agar (A360–500; Fisher Scientific Canada, Ottawa, ON) in deionized water. Iron oxide nanoparticles were added to boiling agar solutions while stirring, and the resulting suspensions were then cooled and poured into 35-mm diameter, 10-mm deep glass Petri dishes. Further cooling to room temperature formed agar gels containing well-dispersed suspensions of nanoparticles, with iron concentrations ranging from 0 to 20 $\mu$g/mL, over which range $\alpha$ remained constant.

## Results

The average output rate over the course of nebulization was 0.70 mg Fe/min. Accordingly, over the 2-hour exposure, 84 mg of iron was introduced into the inhalation chamber. The size distribution of droplets containing the colloidal iron oxide was determined by sampling aerosol from the nose ports of the inhalation chamber. The mass median aerodynamic diameter (MMAD) of the aerosol was 5.6 ± 0.8 $\mu$m, with a geometric standard deviation (GSD) of 1.30 ± 0.03 (both values are expressed as mean ± one standard deviation, $n$ = 6).

In the baseline mice, $T_1$ relaxation times in the right and left lung were measured at different axial positions. Figure 1 displays signal intensity images of 12 axial slices from one of the baseline mice, while Figure 2 demonstrates the use of gray level thresholding to filter out the vasculature from a specified region of interest. In each individual baseline mouse, no variation in the $T_1$ relaxation time was detected with axial position, or between the right and left lung. Therefore, for each mouse, the $T_1$ relaxation time was averaged over the whole lung. As shown in Figure 3, the average $T_1$ relaxation time decreased with the time after death at which the MRI scan was performed. The first and the fifth mouse in this series were exposed to nebulized saline prior to euthanasia, but follow the same trend as do the remaining four baseline mice.

$T_1$ relaxation times in the exposed mice were also determined in the left and right lung, at each of 12 axial positions. Although $T_1$ times varied in different regions of the lungs of the exposed mice, owing to heterogeneous distributions of deposited iron oxide nanoparticles within the lungs, an average value over the entire lung of each mouse was calculated for the sake of comparison with the baseline group. These values are included in Figure 3. A reduction in the average $T_1$ times of the exposed mice from their baseline values is clearly evident in Figure 3. As is expected from Equation (3), under the assumption of similar average lung iron concentrations in each of the exposed mice, this reduction became smaller for the lower baseline $T_1$ times observed with increasing time after death.

For the exposed mice, $T_1$ relaxation times were converted to iron concentrations according to Equation (3). For each mouse, a unique baseline $T_1$ relaxation time, $T_{10}$, was used in Equation (3) to account for the observed decay in $T_{10}$ following death (Fig. 3). $T_{10}$ was determined from the time after death of the mouse by interpolating from the data measured in baseline mice, using a best-fit logarithmic curve. Figure 4 displays average right and left lung iron concentrations in the exposed mice at different axial positions. In each mouse, moving from trachea down to the diaphragm, the first axial slice in which peripheral lung was visible was assigned an axial distance of zero, and the positions of subsequent slices were defined based on their axial distances from the zero position.

The lung volume and total mass of iron deposited in the lung were determined for each exposed mouse based on the number of voxels (each 0.12 × 0.12 × 1 mm in volume) contained in the defined regions of interest in each axial slice and the measured regional iron concentrations. The average lung volume, after thesholding to exclude voxels containing vasculature, was 0.28 ± 0.08 $cm^3$ (mean ± 1 standard deviation, $n$ = 6). The average mass of iron deposited in the lungs was 0.5 ± 0.2 $\mu$g.

## Discussion

In the present work, mice were exposed nose-only to nebulized droplets containing colloidal iron oxide. Concentrations of iron in the lungs of exposed mice were measured using MRI, based on reductions to the $T_1$ relaxation time of the lung tissue, compared to a baseline group of mice. In the baseline mice, the average lung $T_1$ relaxation time was found to decrease with time after death. These changes are most likely due to postmortem redistribution of water between the airway surface liquid, interstitial, and vascular spaces in the lung. In the exposed mice, the concentration of iron was highest in axial slices containing central regions of the lung. This result is not surprising given the sizes of the aerosol droplets in the inhalation chamber, which had a MMAD of 5.6 ± 0.8 $\mu$m. The mathematical lung deposition model presented by Nadithe et al.[12] predicted much higher tracheobronchial deposition than alveolar deposition in mice inhaling particles of several micrometers in diameter. The present results are consistent with this prediction, in that tracheobronchial airways are expected to be located primarily in the central, as opposed to peripheral, regions of the lung.

The total mass of iron that deposited in the lung of each exposed mouse was only 0.0006 ± 0.0002% (mean ± 1 stan-

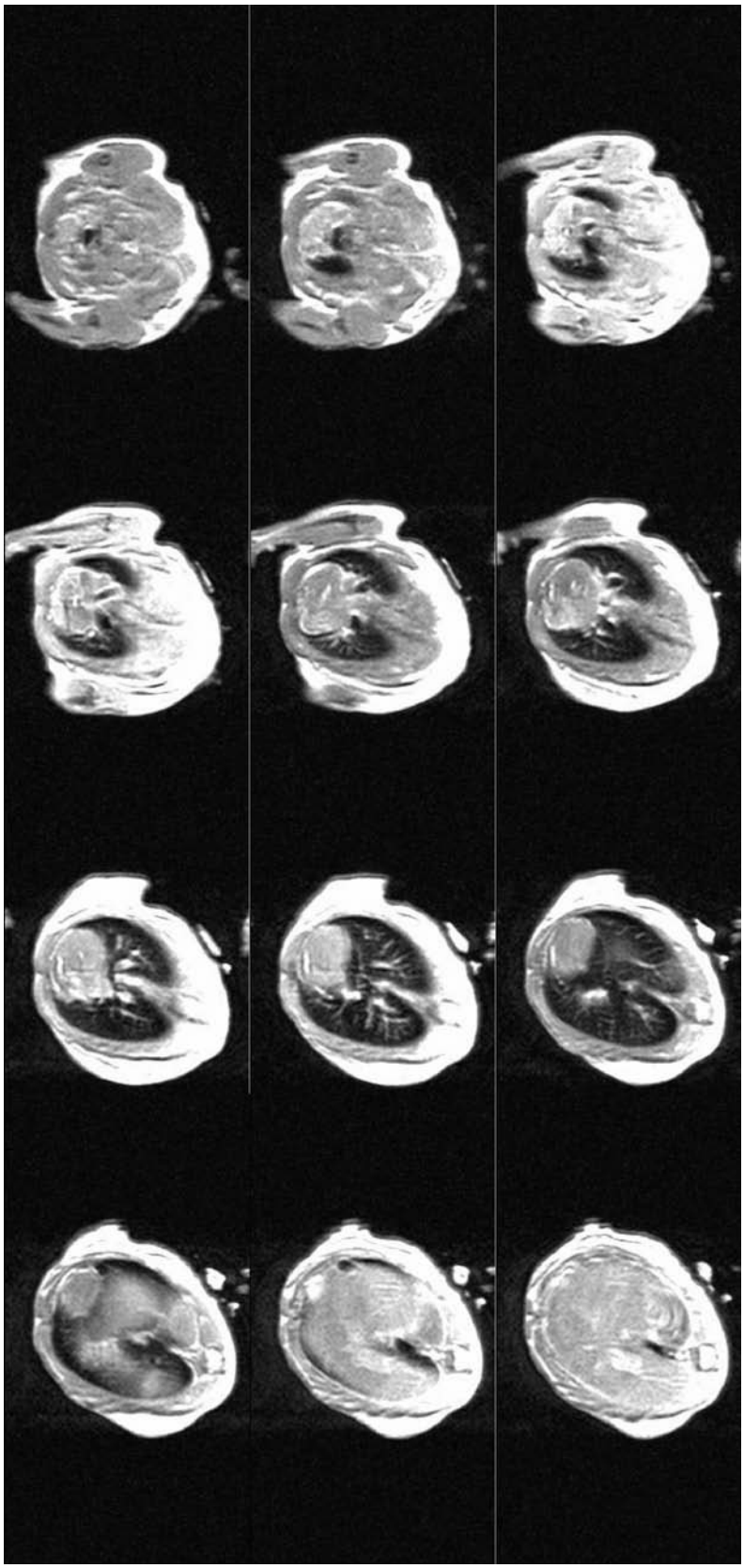

**FIG. 1.** Signal intensity images (for the specific case of no inversion preparation pulse, or $T_i = \infty$) of 12 axial slices of the lung of a baseline mouse, moving from the trachea down to the diaphragm. Each image represents a 1 mm-thick slice. Baseline and exposed mice were indistinguishable in raw signal intensity images such as these.

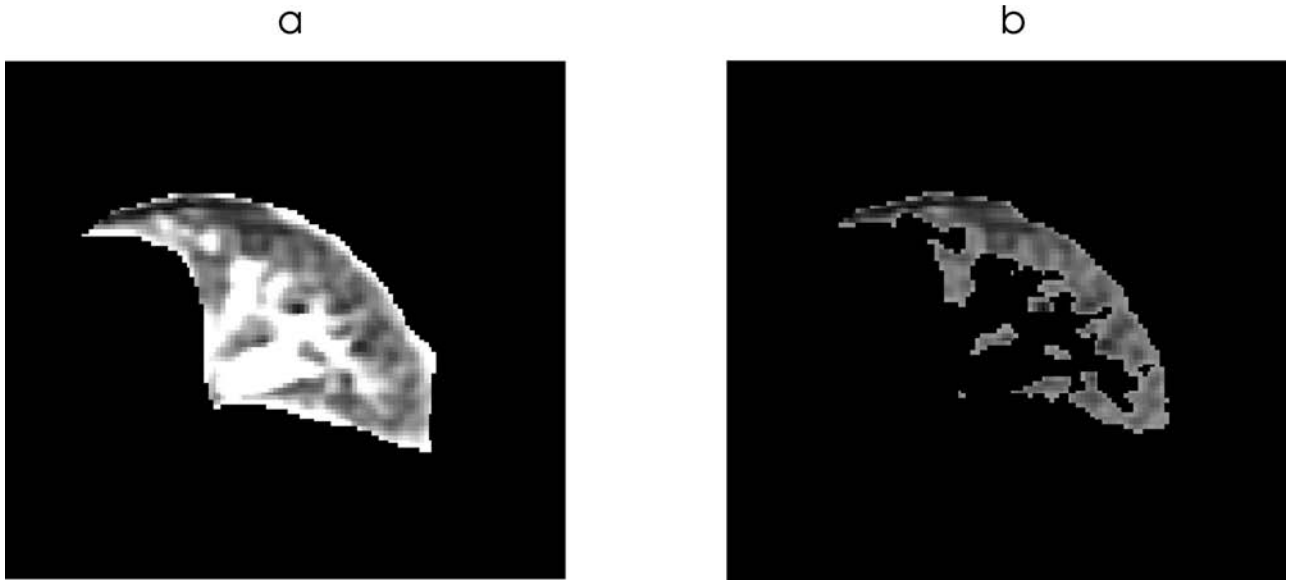


**FIG. 2.** Signal intensity images (for $T_i = \infty$) of a specified region of interest (**a**) before and (**b**) after gray level thresholding to remove the vasculature, which appears as areas of very high intensity in **a.** For the purpose of comparison, the grayscale is held constant between **a** and **b.**

dard deviation, $n = 6$) of the mass of iron introduced into the inhalation chamber. This result is consistent with previous studies, in which nose-only, flow-by inhalation chambers have been shown to be extremely inefficient in terms of the amount of aerosol delivered to the lungs of rodents.[12,15] Employing the same model of nebulizer and compressor, and the identical inhalation chamber as in the present study, Nadithe et al.[12] measured the lung deposition of radiolabeled human serum albumin in mice using gamma scintigraphy. As a percentage of the total activity introduced into the chamber, the average lung deposition in each mouse was 0.0018%. This is three times higher than the lung deposition measured in the present study; however, the reported MMAD of the aerosol was lower than that in the present study, 3.9 $\mu$m compared to 5.6 $\mu$m, so that losses in the chamber, and in the extrathoracic airways of the mice, were likely greater in the present study. In addition, differences in the

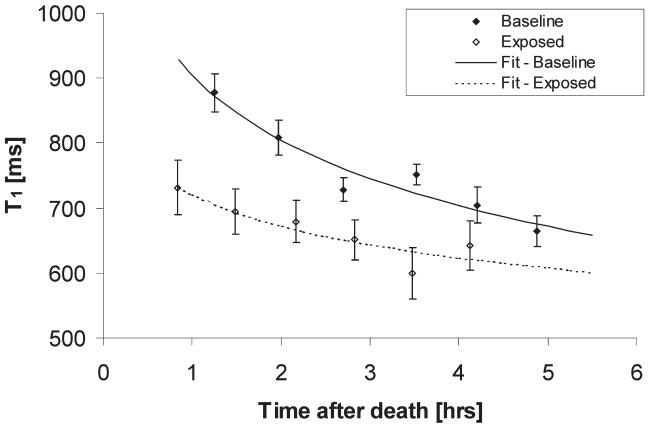


**FIG. 3.** Average $T_1$ relaxation times in the lungs of the baseline and exposed mice are plotted, along with best-fit log-normal curves, against the time after death at which the MRI scan was performed. Error bars represent 95% confidence intervals.

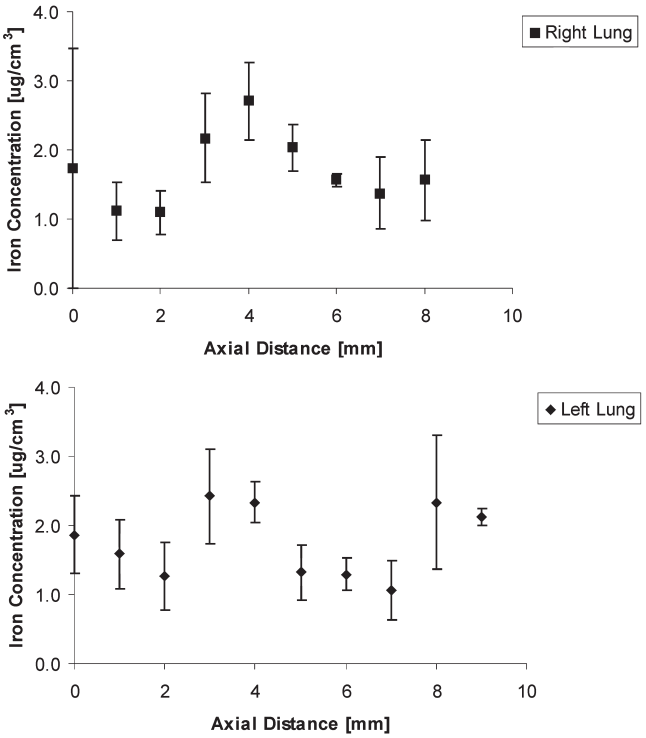


**FIG. 4.** Concentrations of iron in the right and left lung, averaged over the six exposed mice, are plotted against the axial distance, moving from the apex to the base of the lung. Errors bars represent the standard error of the mean.

exposure times and the genetic strains of mice used in the two studies may have contributed to the difference in measured lung deposition.

As was mentioned in the introduction, the ability to quantify regional deposition of superparamagnetic iron oxide nanoparticles within the lung is attractive for *in vivo* evaluation of aerosol-based approaches to magnetic drug targeting. In the present work, separate regions of interest were defined to differentiate between the left and right lung in 1 mm-thick axial slices of the lung. The volume contained within the regions of interest was as small as approximately 2 $mm^3$ for slices at the apex of the lung, but was typically an order of magnitude larger. On average, 16 different regions of interest within the lung were examined for each mouse, with small variation around this average due to the different lung sizes of different mice. While attempts were made to map iron concentrations at finer resolution, within the left and right lung in each slice, the resultant signal to noise ratios were sufficiently low that such mappings were not possible. This is a limitation of the current hardware setup and not an intrinsic limitation of the approach. The MRI scanner used for this study is a whole body human system and thus is not optimized for the study of mice. We therefore expect significant improvements in the ability to detect regional variations in nanoparticle deposition in the study of larger animals and humans. Specifically, it is feasible to use voxel volumes that are 100 to 1000 times larger in a larger animal, which would readily accommodate the analysis of tissue $T_1$ relaxation times at several regions of interest within each lung lobe. $T_1$ mapping in the human lung has been reported by several groups,[16,17] so the technical feasibility of these measurements is well established.

In addition to evaluating regional deposition patterns, MRI measurement of iron concentrations within the lung, and in secondary organs, may be useful for determining clearance rates of insoluble particles *in vivo*. Techniques using gamma scintigraphy[18] are widely used to measure short-term, mucociliary clearance over 24 h. The observation time in these studies is limited by the short half-life of the radiolabel, usually technetium-99m. In limited cases, clearance has been measured by scintigraphy over several days, and even months, using radiolabels with longer half-life and sensitive counters.[19,20] Alternatively, Möller et al.[21,22] measured whole-lung retention of inhaled micrometer-sized iron oxide particles over a time period of 9 months, using a superconducting quantum interference device (SQUID) to detect remanent magnetic fields produced by magnetized particles. Similar studies may be possible using MRI after inhalation of superparamagnetic iron oxide nanoparticles, or larger insoluble particles labeled with a MRI contrast agent, with the added benefit of obtaining regional deposition patterns. If such studies are undertaken, a potential limiting factor is the sensitivity of the $T_1$ relaxation time of the lung, and of secondary organs, to the tissue concentration of contrast agent. This sensitivity is captured in the parameter $\alpha$, in Equation (3). In the present work, iron concentrations in the lung on the order of 1 $\mu g/cm^3$ were successfully measured. Following Equation (3), for the superparamagnetic iron oxide preparation used in the present study, an iron concentration of 1 $\mu g/cm^3$ in the lung decreases a baseline $T_1$ relaxation time of 800 ms to 714 ms. Smaller concentrations would have been difficult to detect in the present work, as changes to the $T_1$ relaxation time would have been of the same magnitude as the experimental error in the measurements.

In summary, based on the work described above, it can be concluded that MRI measurement of $T_1$ relaxation times shows considerable promise as an experimental technique for determining regional lung deposition of inhaled superparamagnetic iron oxide particles. Such a technique is well suited for evaluation of aerosol-based magnetic drug targeting to localized sites within the lung, where drug or carrier particles are already loaded with iron oxide nanoparticles to increase their magnetic susceptibilities. In addition, as an alternative to scintigraphy, MRI may prove useful in determining particle concentrations in the lung during long-term clearance studies

## Acknowledgments

A.M. acknowledges financial support in the form of student scholarships from the Natural Sciences and Engineering Research Council of Canada, the Alberta Ingenuity Fund, and the Killam Fund. W.H.F. gratefully acknowledges research funding from the Natural Sciences and Engineering Research Council of Canada, and Alberta Advanced Education and Technology. In planning the animal exposure, the authors benefited greatly from discussions with Dr. Toni Bayans, Dr. Greg Parks, and Dr. Michael Oldham. In addition, the authors thank Nicole Olivier for providing technical expertise and assistance in all animal procedures.

## Author Disclosure Statement

The authors disclose that no conflicting financial interests exist.

## References

1. Coates AL: Guiding aerosol deposition in the lung. N Engl J Med. 2008;358:304–305.
2. Plank C: Nanomagnetosols: magnetism opens up new perspectives for targeted aerosol delivery to the lung. Trends Biotechnol. 2008;26:59-63.
3. Dames P, Gleich B, Flemmer A, Hajek K, Seidl N, Wiekhorst F, Eberbeck D, Bittmann I, Bergemann C, Weyh T, Trahms L, Rosenecker J, and Rudolph C: Targeted delivery of magnetic aerosol droplets to the lung. Nat Nanotechnol. 2007;2:495–499.
4. Martin AR, and Finlay WH: Alignment of magnetite loaded high aspect ratio aerosol drug particles with magnetic fields. Aerosol Sci Technol. 2008;42:245–248.
5. Shang YH, Finlay WH, and Moussa WA: Numerical analysis of thermally induced micro fiber deformation using a high frequency magnetic field in human lung. J Comp Theor Nanosci 2008;5:294–301.
6. Weinmann H-J, Ebert W, Misselwitz B, and Schmitt-Willich H: Tissure-specific MR contrast agents. Eur J Radiol. 2003;46:33–44.
7. Bellin M-F. MR contrast agents, the old and the new. Eur J Radiol 2006;60:314–323.
8. Lemke A-J, von Pilsach MIS, Lubbe A, Bergemann C, Riess H, and Felix R: MRI after magnetic drug targeting in patients with advanced solid malignant tumors. Eur Radiol. 2004;14:1949–1955.
9. Chertok B, Moffat BA, David AE, Yu F, Bergemann C, Ross BD, and Yang VC: Iron oxide nanoparticles as a drug de-

livery vehicle for MRI monitored magnetic targeting of brain tumors. Biomaterials. 2008;29:487–496.
10. Sood BG, Shen Y, Latif Z, Chen X, Sharp J, Neelavalli J, Joshi A, Slovis TL, and Haacke EM: Aerosol delivery in ventilated newborn pigs: an MRI evaluation. Pediatr Res. in press.
11. Phalen RF, Oldham MJ, and Wolff RK: The relevance of animal models for aerosol studies. J Aerosol Med. 2008;21:113–124.
12. Nadithe V, Rahamatalla M, Finlay WH, Mercer JR, and Samuel J: Evaluation of nose-only aerosol inhalation chamber and comparison of experimental results with mathematical simulation of aerosol deposition in mouse lungs. J Pharm Sci. 2003;92:1066–1076.
13. Rosenthal SG, Willich HC, Ebert W, and Conrad J: The demonstration of human tumors on nude mice using gadolinium-labeled monoclonal antibodies for magnetic resonance imaging. Invest Radiol. 1993;28:789-793.
14. Suwa T, Ozawa S, Ueda M, Ando N, and Kitajima M: Magnetic resonance imaging of esophageal squamous cell carcinoma using magnetite particles coated with anti-epidermal growth factor receptor antibody. Int J Cancer. 1998;75: 626–634.
15. Costa DL, Lehmann JR, Winsett D, Richards J, Ledbetter AD, and Dreher KL: Comparative pulmonary toxicological assessment of oil combustion particles following inhalation or instillation exposure. Toxicol Sci. 2006;91:237–246.
16. Arnold JFT, Fidler F, Wang T, Pracht ED, Schmidt M, and Jakob PM: Imaging lung function using rapid dynamic acquisition of $T_1$-maps during oxygen enhancement. MAGMA. 2004;16:246–253.
17. Stadler A, Jakob PM, Griswold M, Stiebellehner L, Barth M, and Bankier AA: $T_1$ mapping of the entire lung parenchyma: Influence of respiratory phase and correlation to lung function test results in patients with diffuse lung disease. Magn. Reson. Med. 008;59:96–101.
18. Fleming JS, Quint M, Bolt L, Martonen TB, and Conway JH: Comparison of SPECT aerosol deposition data with twenty-four-hour clearance measurements. J Aerosol Med. 2006;19: 261–267.
19. Lindstrom M, Camner P, Falk R, Hjelte L, Philipson K, and Svartengren M: Long-term clearance from small airways in patients with cystic fibrosis. Eur Respir J. 2005;25:317–323.
20. Falk R, Philipson K, Svartengren M, Bergmann R, Hofmann W, Jarvis N, Bailey M, and Camner P: Assesment of long-term bronchiolar clearance of particles from measurements of lung retention and theoretical estimates of regional deposition. Exp Lung Res. 1999;25:495–516.
21. Möller W, Häubinger K, Winkler-Heil R, Stahlhofen W, Meyer T, Hofmann W, and Heyder J: Mucociliary and long-term particle clearance in the airways of healthy nonsmoker subjects. J Appl Physiol. 2004;97:2200–2206.
22. Möller W, Häubinger K, Ziegler-Heitbrock L, and Heyder J: Mucociliary and long-term particle clearance in airways of patients with immotile cilia. Respir Res. 2006;7:10.

Received April 6, 2008
in final form, June 25, 2008

Reviewed by:
Theresa Sweeney
Allan Coates

Address reprint requests to:
*Warren H. Finlay, Ph.D.*
*Deparrtment of Mechanical Eng.*
*University of Alberta*
*Edmonton, AB T6G 2G8, Canada*

*E-mail:* warren.finlay@ualberta.ca